Journal of Materials Chemistry A

Accepted Manuscript

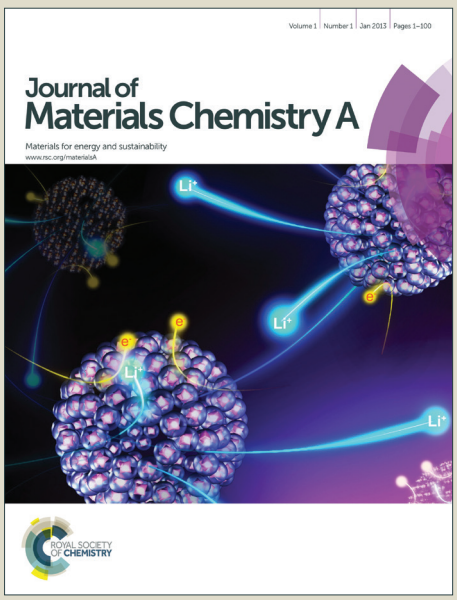

ROYAL SOCIETY OF CHEMISTRY

www.rsc.org/materialsA

Three-Dimensional and Stable Polyaniline-Grafted Graphene Hybrid Materials for Supercapacitor Electrodes

Xianbin Liu, Pengbo Shang, Yanbing Zhang, Xiaoli Wang,

Zhimin Fan, Bingxi Wang, Yuying Zheng*

College of Materials Science and Engineering, Fuzhou University, Fuzhou, 350116, China

* Corresponding author. Fax: (+86) 591 22866529.

E-mail address: yyzheng@fzu.edu.cn

Abstract:

A novel route was introduced to synthesize hierarchical polyaniline-grafted reduced graphene oxide (rGO) hybrid materials by polyaniline nanorods covalently bonded on the surface of rGO. Aminophenyl groups were initially grafted on rGO via diazonium treatment. Then the PANI nanorods were aligned vertically on the rGO to construct a three-dimensional (3D) structure. The 3D structure could shorten the electronic transmission path and form abundant space for electrolyte ions. The hybrid materials fabricated as supercapacitor electrode exhibited a maximal specific capacitance of 1045.51F/g, and the energy density (E) could achieve an upper value of 8.3 Wh/kg at the current density of 0.2 A/g simultaneously. Such a highly stable three-dimensional structural hybrid materials is very promising for the next high-performance electrochemical supercapacitors.

Key word: covalent bond; polyaniline nanorods; reduced graphene oxide; supercapacitors.

1 Introduction

Supercapacitors have attracted intense interest as ideal energy storage devices for applications such as laptops, cell phone, etc[1-6]. Since graphene, consisting of a single layer carbon, was prepared by Konstantin Novoselov in 2004, it has been regarded as a potential electrode for electrochemical double layer capacitors (EDLCs) due to its unique properties such as large surface area, good electronic conductivity and high electrochemical stability[7-10]. The theoretical special surface area of two-dimensional graphene is 2630 m^2/g and the interface capacitance is found to be 21μF/cm^2, implying a maximum electrochemical double-layer capacitance of 550 F/g[11-13]. However, the present graphene could not meet the demand of high energy and power densities on account of unavoidably aggregating and the limited capacitance of electrochemical double layer capacitors[14]. Therefore, it is extremely necessary to combine the metal oxides[15-19] or conductive polymers[12, 20, 21] based on faradic pseudocapacitance with graphene, even both the metal oxides and conductive polymers[22].

Polyaniline, possessing a large theoretical pseudocapacitance, good chemical stability, and low cost combined with the easiness of preparation[23, 24], has been considered as a promising object composited with graphene. In the previous reports[20, 25-28], most of the PANI/graphene composite materials were interconnected by Van der Waals force and hydrogen bond. By contrast, the covalent bond is more conductive to enhance the electrical conductivity and stability of composites. To date, most of covalent connection in the PANI/graphene composite materials were based on the functional groups of GO[21, 29, 30]. However, the functional groups on the double faces of graphene are limited. More importantly, the linkage was not π-conjugated molecular chain limited the overall conductivity of the composite. Therefore, the striving to enhance the synergistic effect between PANI and graphene to improve overall performance of PNAI/graphene composite is still needed.

In this paper, we reported a feasible route to prepare polyaniline-grafted reduced graphene oxide hybrid materials. The aminophenyl diazonium salts were firstly synthesized by using ion exchange resins, following reacted with reduction graphene

oxide to prepare 4-aminophenyl grafted reduced graphene oxide. After that, the PANI nanorods were arranged vertically in the double faces of graphene via covalent connection. With the synergistic effect of two-dimensional graphene and one-dimensional PANI nanorods, The PANI/rGO composites display highly ordered so that the PANI/rGO composite electrode showed good electrochemical properties.

2 Experiments

2.1 Material

Natural graphite powder (99.995%, 300 mesh) was supplied by Institute of Shenghua (Changsha, China). All other reagents were purchased from Sinopharm Chemical Reagent Company (Shanghai, China). Aniline was distilled twice under reduced pressure and other reagents were used as received without further treatment.

2.2 4-aminophenyl grafted reduced graphene oxide (rGO-NH_2)

The graphene oxide (GO) was firstly prepared by improved-hummer method[31]. GO (100mg) was dispersed in 100 mL ultrapure water by ultrasonic treatment for 1 h, 30 μL $NH_3 \cdot H_2O$ and 30 μL hydrazine were then added into the solution to reduce the GO. rGO-NH_2 was obtained by diazotization reaction[32-34]. The mixture was reacted for 24 h. And lastly, the product was washed thoroughly by ultrapure water and vacuum dried at 80 ^oC.

2.3 Polyaniline grafted reduced graphene oxide composites

The polyaniline grafted reduced graphene oxide composites were prepared by low temperature oxidation polymerization method. Briefly, 36 mg rGO-NH_2 was dispersed in 100 mL $HClO_4$ solution (1 mol/L) with ultrasonic treatment for 1 h, and the mixed solution was then placed at -10 ^oC for uniform nucleation. In order to prevent the solution being frozen, 25 mL ethanol was added. Subsequently, different concentrations of aniline (0.01 mol/L, 0.02 mol/L, 0.05 mol/L) and corresponding ammonium persulfate (3:2 molar ratio of aniline to APS) were added into above solution dropwise separately. After reacted for 24 h, the product was obtained by filtering and finally drying at 60 ^oC for 24 h.

2.4 Characterization

Atomic force microscopy (AFM) images were obtained with Agilent 5500 (USA) using a tapping mode. Transmission electron microscopy (TEM) was performed on a a Tecnai G2F20 (FEI, USA). The scanning electron microscopy analysis was taken using a Nova Nano SEM 230 (FEI, Holland) with Inlens detector at 2kV. Fourier transform infrared spectroscopy (Thermo Nicolet5700, USA) and Raman spectroscopy (Renishaw Invia, UK) were used to analyze the chemical structure of products. All electrochemical experiments were carried out on an electrochemical workstation (CHI 660D, Shanghai Chenhua) with a three-electrode system in 1 M H_2SO_4 electrolyte. 2 mg of sample was dispersed in1 mL of ethanol containing 10 μL Nafion solution (5 % in water) to form a mixed suspension. The working electrode was prepared by droping the mixed suspension onto a pretreated glassy carbon electrode (Φ=3 mm) by polishing, ultrasonic cleaning. Pt sheet worked as the counter electrode and Ag/AgCl as the reference electrode. The asymmetric supercapacitor was tested in a two-electrode device, the working electrode was prepared with 85 wt% active material, 10 wt% acetylene black and 5 wt% PTFE emulsion, active carbon was directly used as counter electrode. And the 1 mol/L H_2SO_4 aqueous solution was used as electrolyte.

3 Results

3.1 Morphology and Structure

The graphene oxide prepared by improved-hummer method was analyzed by atomic force microscopy (AFM). As shown in Fig 1a, the thickness of the GO was about 1.0 nm, similar to the previous report[31]. Additionally the size was 1 to 2 μm, providing a large template for PANI growing. The 3D topography of PANI/rGO was shown in Fig.1b. It was easily found that the PANI nanorods were grown vertically on the surface of rGO nanosheets. The SEM (Fig.1c) image showed that the nanorods were well-aligned arranging with several ten nanometers in length and could form plenty of space, which could accelerate the electronic transmission and allow the electrolyte ions to enter. In addition, the diameter of nanorods with approximately 30 nm was estimated through the TEM (Fig.1d) image.

For such a unique structure, it was extremely attractive to explore the formation mechanism. Therefore, a series of PANI/rGO composites were prepared at different reaction time and aniline concentrations, Fig.2a-c were the SEM images of PANI/rGO composites polymerized at the reaction time of 3 h, 6 h, and 18 h, respectively. As shown in Fig.2a, only a few PANI nanorods were grown on the rGO surfaces and the length very short. As the reaction time increased to 18 h, a large amount of PANI nanorods were clearly visible in Fig.2c, In general, the aniline monomers tend to heterogeneous nucleation on the surface of graphene nanosheets in suit polymerization. Therefore, the graphene were easily wrapped by PANI initially. However, Aminophenyl groups were introduced to induce homogenous nucleation of aniline[28], and a few PANI nanorods were grown. With the reaction time increased, most monomers tend to homogenous nucleation and form the ordered nanorods. At the end, the PANI molecular chains became longer and the nanorods were gradually grown. The same results could be concluded by Fig.2d-f with the effect of monomer concentration. At a low concentration of 0.01 mol/L, most of the aniline monomers were tends to heterogeneous nucleation to form cladding layer. As the concentration increased, more and more monomers were polymerized to homogeneous nucleation. The length of PANI nanorods was becoming more and more long.

In order to confirm the functional group and PANI on the faces of rGO, Fourier transform infrared spectroscopy (FT-IR) was carried out to characterize the chemical structure. As shown in Fig.2a, the spectrum of GO showed absorption at 1720cm^{-1}, 1390 cm^{-1},1260 cm^{-1} and 1110 cm^{-1} which were ascribed to the vibration of C=O, C-O in COOH, C-O-C and C-OH, respectively. The sharp band at 1625 cm^{-1} was attributed to the residual water. The second curve of spectrum displayed new bands at 3460 cm^{-1}, 1646 cm^{-1}, 1408 cm^{-1} and 1302 cm^{-1}, which were the characteristic peaks of aminophenyl group, and the 1060 cm^{-1} corresponding to the C-N stretching generated by diazotization, confirmed that aminophenyl groups had been successfully grafted on the surface of rGO. Two characteristic peaks at 1565 cm^{-1} and 1467 cm^{-1} were attributed to the absorbance of C=C stretching deformations of quinonoid and benzenoid ring, clearly demonstrating that PANI was grown on the rGO. Moreover,

the peaks at 1278 cm^{-1}, 1232 cm^{-1} and 811 cm^{-1} were due to the absorption of C-N, C=N and C-H stretching. The band at 1125 cm^{-1} was red-shifted from original 1150cm^{-1}, caused by H^+ doping in quinonoid ring. And the conductivity of PANI was highly improved.

Raman spectrum analysis was used to explain a more precise chemical structure. In the Fig.2b, the spectrum of GO and rGO displayed two prominent peaks at 1319 cm^{-1} and 1592 cm^{-1} which were corresponded to D mode and G mode., representing the conversion of a sp^2-hybridized to a sp^3-hybridized and the in-plane vibration of sp^2-hybridized. The intensity ratio (D/G) suggests the defect content and order degree. It was worth noting that the ratio of rGO was increased along the chemical reduction reaction, while the ratio of PANI/rGO was decreased in comparison with that of both GO and rGO. This might be due to the ordering of graphene improved by vertically arranged PANI nanorods. Particularly, the D band of PANI/rGO shifts from 1319 to 1326 cm^{-1} because of the strong interaction. In addition, the reappearance of bands at 1176cm^{-1}, 1228 cm^{-1}, 1385 cm^{-1}, 1465 cm^{-1} indicated the PANI was grown on the face of rGO. All of these evidences pointed out that the PANI nanorods had been successfully grafted onto the surface of rGO.

3.2 Electrochemical property

In order to explore their application as supercapacitor electrodes, the electrochemical performances of PANI/rGO composites were tested by cyclic voltammetry (CV), galvanostatic charge/discharge and electrochemical impedance spectroscopy (EIS). As shown in Fig.4a, two pairs of conspicuous peaks were appeared in the CV curses, which were attributed to the two redox transitions of PANI containing leucoemeraldine-emeraldine transformation and emeraldine to pernigranilne[35]. Therefore, the capacitance of the composite mainly was generated by redox reactions of PANI. The effect of scan rate on the CV was also investigated from 5 to 200 mV/s. The nearly linear increase of the peak current density showed a good rate performance of PANI/rGO.

To further affirm the superior property of the PANI/rGO composite, the CV curve of pure PANI, rGO were investigated to compare with PANI/rGO in the Fig.4b.

It was obviously seen that the PANI/rGO composite possessed the highest peak current when the aniline concentration was 0.05 mol/L. The results suggested that the 3D uniform structure greatly promoted the capacitance of PANI/rGO hybrid materials.

The specific capacitance (C_s, F/g) was calculated according to the following equation:

$$C_s = \frac{I\Delta t}{\Delta V \times m}$$

Where I (A), Δt (s) and ΔV (V) are the discharge current, time and potential window in the charge/discharge curve, and m (g) is the mass of the active material. As shown in Fig.4c, the almost symmetric charge-discharge curves showed a good capacitive behavior at large-scale current densities. The capacitance was up to 1045.51 F/g at 0.2 A/g. With the current density increasing to 5 A/g, the specific capacitance was still 338.67 F/g, which was attributed to the fact that the redox reaction rate and charge diffusion could not keep pace with the rapid change of potential. The grafted Aminophenyl groups as a anchor impel the PANI nanorods growing regularly, so that more electrolyte ions could aggregate on the electrode/electrolyte surface.

The charge/discharge curves of PANI/rGO composites prepared at different aniline concentration, pure PANI and rGO were revealed in Fig.4d. It was clearly seen that the "IR" of PANI/rGO at the aniline concentration as 0.05 mol/L was the smallest, signifying the lowest internal resistance of the electrode. This result could be explained by the following factors. First, the covalent connection reduces the interface resistance between the PANI molecular chains and graphene sheets and the forming of π-conjugated structure enhances the electron transport. Second, the raised PANI nanorods shorten electrolyte ions transmission paths. Second, the covalent connection between the PANI molecular chains and graphene sheets reduces the interface resistance and enhances the electron transport, and the longer in length, the better electrical conductivity.

Cycling performance was carried out at the current density of 1 A/g. As shown in Fig.4e, PANI/rGO presented excellent cycling stability and the specific capacitance retained 94.8%, much higher than the pure PANI (89.2%) and other PANI-rGO

composites prepared by noncovalent-bond connected[15-21]. Meanwhile, the composite electrodes have been performed for 10000 cycles at a scan rate of 100 mV/s. The specific capacitance still maintained 85.3% as the inset in Fig.4e. It was well known that PANI suffered from a limited stability of cycling due to the destruction of molecular structure during the oxidation-reduction process, therefore, when the PANI molecular chains were fastened on the surface of rGO as a substrate via covalent band, the stability of PANI could be sharply enhanced.

The electrochemical impedance spectroscopy (EIS) was tested in the frequency range of 10^5 to 10^{-2} Hz. As shown in Fig.4f, the Nyquist plots of PANI/rGO and pure PANI were an incomplete semicircle in the high-frequency region and a straight line in the low-frequency region. The intercepts of the curves with real impedance axis, mainly indicating the contact resistance at the interface of active material/current collector, were about 6.2 and 10.3 ohm, respectively. The interfacial charge-transfer resistance (R_{ct}) was calculated by the diameter of semicircle[36, 37]. The R_{ct} of the PANI/rGO was 2.6 ohm, smaller than the pure PANI (3.1 ohm). The long uniform nanorods accelerated transformation of the charge. The Nyquist plots could be modeled by a complex equivalent circuit, as shown by the inset in Fig.4f. The R_s was in series to the C. The C_d and C_f represented electrochemical double layer capacitance and faradic capacitance separately. The R_{ict} was the charge transfer resistance at the electrode/electrolyte interface because of the different wettability, while R_{ect} was the electron transfer resistance at the redox reaction.

To evaluate further the supercapacitor performance of the PANI/rGO hybrid material, the energy density (E) and power density (P) were calculated based on the asymmetric supercapacitor. The Ragone plot was shown in Fig.5, the maximum energy density was 8.3 Wh/kg at the current density of 0.2 A/g, meanwhile the power density could up to a value of 60 kW/kg. It was inferred that the PANI/rGO composite electrode could meet the demand of high energy density and power density simultaneously[].

4 Conclusions

In summary, a novel route for fabricating 3D stable PANI/rGO hybrid materials was reported. By employing the aminophenyl groups as anchors, PANI nanorods were successfully grown on the double faces of reduced graphene oxide nanosheets. The morphologies of hybrid material could be controlled by the aniline concentration and reaction time. With an optimal condition, the specific capacitance could reach up to 1045.51 F/g at 0.2 A/g. The energy density (E) and power density (P) was 8.3 Wh/kg and 60 kW/kg at the same time. Besides PANI/rGO composites presented excellent durability and the specific capacitance could retain 94.8%. The superior electrochemical performance was attributed to the 3D nanorods and covalent-bond structure. This unique 3D structural material can be used as a promising kind of electrode in the next high energy density and high power density electrochemical supercapacitors[38].

Acknowledgements

This work was supported by Scientific and Technological Innovation Project of Fujian Province (Grant No. 2012H6008), Scientific and Technological Innovation Project of Fuzhou City (Grant No. 2013-G-92).

References

[1] B. Conway, *Scientific Fundamentals and Technological Applications, Kluwer Academic/Plenum Publishers, New York*, 1999.

[2] H. Y. Lee and J. B. Goodenough, *J. Solid State Chem.* 1999, **144**, 220-223.

[3] X. Liu, D. Wu, H. Wang and Q. Wang, *Adv. Mater.* 2014, **26**, 4370-4375.

[4] Y. Sun, Q. Wu and G. Shi, *Energy Environ. Sci.* 2011, **4**, 1113-1132.

[5] L. Zhao, L. Z. Fan, M. Q. Zhou, H. Guan, S. Qiao, M. Antonietti and M. M. Titirici, *Adv. Mater.* 2010, **22**, 5202-5206.

[6] A. Thomas, P. Kuhn, J. Weber, M. M. Titirici and M. Antonietti, *Macromol. Rapid Commun.* 2009, **30**, 221-236.

[7] M. J. Allen, V. C. Tung and R. B. Kaner, *Chem. Rev.*, 2009, **110**, 132-145.

[8] Y. B. Tan and J. M. Lee, *J. Mater. Chem. A*. 2013, **1**, 14814-14843.

[9] C. Liu, Z. Yu, D. Neff, A. Zhamu and B. Z. Jang, *Nano Lett.* 2010, **10**, 4863-4868.

[10] L. H. Kumar, C. V. Rao and B. Viswanathan, *J. Mater. Chem. A.* 2013, **1**, 3355-3361.

[11] M. F. El-Kady, V. Strong, S. Dubin and R. B. Kaner, *Science*, 2012, **335**, 1326-1330.

[12] M. D. Stoller, S. Park, Y. Zhu, J. An and R. S. Ruoff, *Nano Lett.* 2008, **8**, 3498-3502.

[13] L. Zhang and G. Shi, *J. Phys. Chem. C.* 2011, **115**, 17206-17212.

[14] D. Pech, M. Brunet, H. Durou, P. Huang, V. Mochalin, Y. Gogotsi, P.-L. Taberna and P. Simon, *Nat. Nanotechn.* 2010, **5**, 651-654.

[15] M. Pumera, *Energy Environ. Sci.* 2011, **4**, 668-674.

[16] Z.-S. Wu, G. Zhou, L.-C. Yin, W. Ren, F. Li and H.-M. Cheng, *Nano Energy*, 2012, **1**, 107-131.

[17] S. Chen, J. Zhu, X. Wu, Q. Han and X. Wang, *ACS Nano*, 2010, **4**, 2822-2830.

[18] W. Zhou, J. Liu, T. Chen, K. S. Tan, X. Jia, Z. Luo, C. Cong, H. Yang, C. M. Li and T. Yu, *Phys. Chem. Chem. Phys.* 2011, **13**, 14462-14465.

[19] U. M. Patil, J. S. Sohn, S. B. Kulkarni, H. G. Park, Y. Jung, K. V. Gurav, J. H. Kim and S. C. Jun, *Mater. Lett.* 2014, **119**, 135-139.

[20] K. Zhang, L. L. Zhang, X. Zhao and J. Wu, *Chem. Mater.* 2010, **22**, 1392-1401.

[21] N. A. Kumar, H. J. Choi, Y. R. Shin, D. W. Chang, L. Dai and J. B. Baek, *ACS Nano*, 2012, **6**, 1715-1723.

[22] G. Yu, L. Hu, N. Liu, H. Wang, M. Vosgueritchian, Y. Yang, Y. Cui and Z. Bao, *Nano Lett.* 2011, **11**, 4438-4442.

[23] X. Yan, J. Chen, J. Yang, Q. Xue and P. Miele, *ACS Appl. Mater. Interfaces*, 2010, **2**, 2521-2529.

[24] D. Li, J. Huang and R. B. Kaner, *Acc. Chem. Res.* 2008, **42**, 135-145.

[25] S. B. Kulkarni, U. M. Patil, I. Shackery, J. S. Sohn, S. Lee, B. Park and S. Jun, *J. Mater. Chem. A.* 2014, **2**, 4989-4998.

[26] Z. F. Li, H. Zhang, Q. Liu, L. Sun, L. Stanciu and J. Xie, *ACS Appl. Mater. Interfaces.* 2013, **5**, 2685-2691.

[27] J. Xu, K. Wang, S. Z. Zu, B. H. Han and Z. Wei, *ACS Nano*, 2010, **4**, 5019-5026.

[28] J. Yan, T. Wei, B. Shao, Z. Fan, W. Qian, M. Zhang and F. Wei, *Carbon*, 2010, **48**, 487-493.

[29] J. An, J. Liu, Y. Zhou, H. Zhao, Y. Ma, M. Li, M. Yu and S. Li, *J. Phys. Chem. C*, 2012, **116**, 19699-19708.

[30] L. Jianhua, A. Junwei, Z. Yecheng, M. Yuxiao, L. Mengliu, Y. Mei and L. Songmei, *ACS Appl. Mater. Interfaces* 2012, **4**, 2870-2876.

[31] D. C. Marcano, D. V. Kosynkin, J. M. Berlin, A. Sinitskii, Z. Sun, A. Slesarev, L. B. Alemany, W.

Lu and J. M. Tour, *ACS Nano*, 2010, **4**, 4806-4814.

[32] V. D. Filimonov, M. Trusova, P. Postnikov, E. A. Krasnokutskaya, Y. M. Lee, H. Y. Hwang, H. Kim and K. W. Chi, *Org. Lett.* 2008, **10**, 3961-3964.

[33] T. He, D. A. Corley, M. Lu, N. H. D. Spigna, J. He, D. P. Nackashi, P. D. Franzon and J. M. Tour, *J. Am. Chem. Soc.* 2009, **131**, 10023-10030.

[34] Y. Zhu and J. M. Tour, *Nano Lett.* 2010, **10**, 4356-4362.

[35] Q. Wu, Y. Xu, Z. Yao, A. Liu and G. Shi, *Acs Nano*, 2010, **4**, 1963-1970.

[36] J. Rajeswari, P. S. Kishore, B. Viswanathan and T. K. Varadarajan, *Electrochem. Commun.* 2009, **11**, 572-575.

[37] X. Li, J. Rong and B. Wei, *ACS Nano*, 2010, **4**, 6039-6049.

[38] X. Liu, Z. Wen, D. Wu, H. Wang, J. Yang and Q. Wang, *J. Mater. Chem. A*, 2014, **2**, 11569-11573.

Figure caption

Fig.1 (a) AFM image of GO; (b) AFM, (c) SEM, and (d) TEM images of PANI/rGO.

Fig.2 SEM image of PANI/rGO composites at different reaction time: of (a) 3 h; (b) 6h; (c) 18 h and different aniline monomer concentration of (d) 0.01 mol/L; (e) 0.02 mol/L; (f) 0.05 mol/L.

Fig.3 (a) FTIR spectrum of GO, rGO-NH_2 and PANI/rGO; (b) Raman spectrum of GO, rGO, pure PANI and PANI/rGO.

Fig.4 (a) CV of PANI/rGO at different scan rates; (b) CV of rGO, pure PANI and PANI/rGO at different monomer concentrations at scan rate of 100 mV/s; (c) charge/discharge curves of PANI/rGO at different current densities; (d) charge/discharge curves of rGO, pure PANI and PANI/rGO at 1A/g; (e) cycling performance of PANI/rGO at 1 A/g for 1000 cycles and 100 mV/s for 10000 cycles; (d) EIS of the PANI and PANI/rGO.

Fig.5 The Ragone plot of energy density versus power density for the PANI/rGO at different charge/discharge current densities.

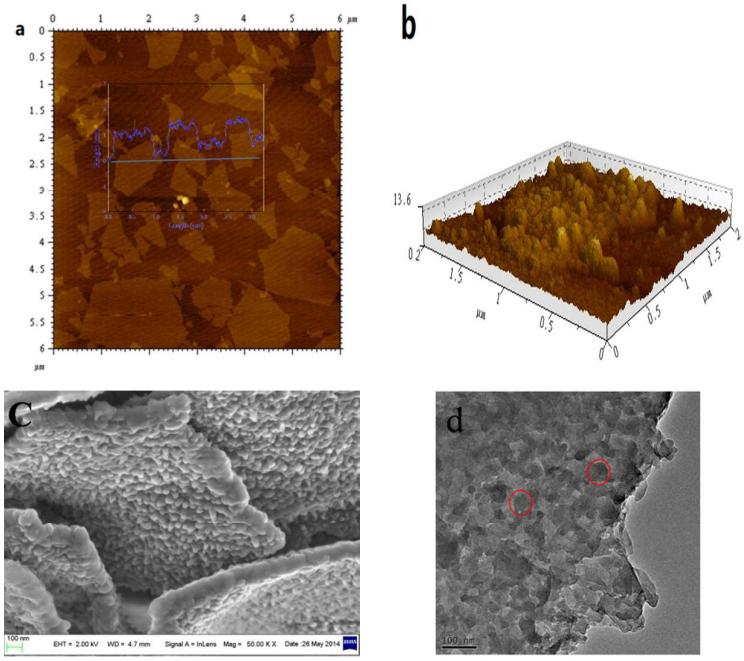

Fig.1 (a) AFM image of GO; (b) AFM, (c) SEM and (d) TEM images of PANI/rGO.

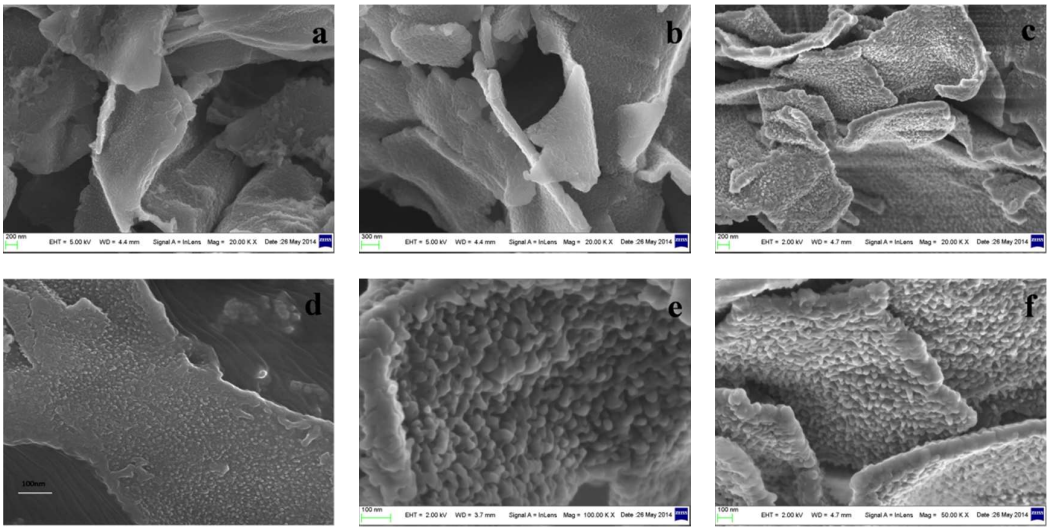

Fig.2 SEM images of PANI/rGO composites at different reaction time: of (a) 3 h; (b) 6 h; (c) 18 h and different aniline monomer concentration of (d) 0.01 mol/L; (e) 0.02 mol/L; (f) 0.05 mol/L.

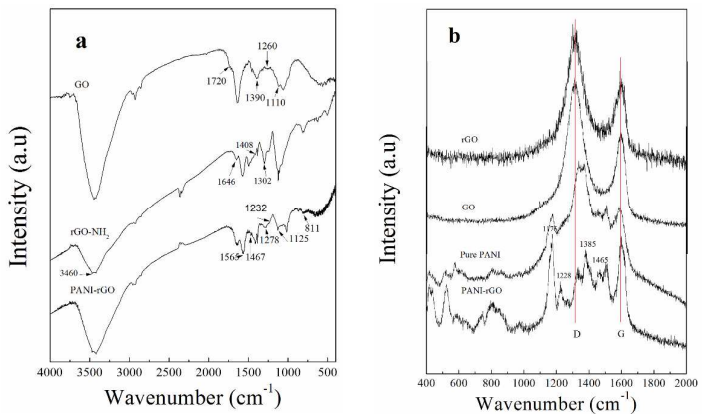

Fig.3 (a) FTIR spectrums of GO, rGO-NH_2 and PANI/rGO; (b) Raman spectrums of GO, rGO, pure PANI and PANI/rGO.

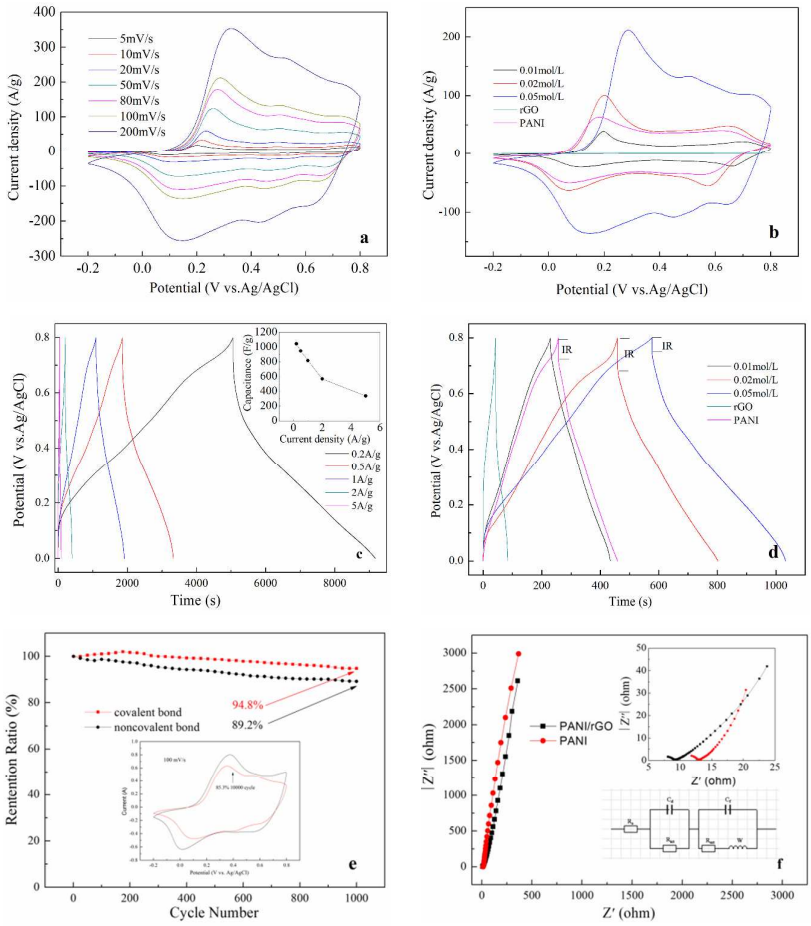

Fig.4 (a) CV of PANI/rGO at different scan rates; (b) CV of rGO, pure PANI and PANI/rGO at different monomer concentration at scan rate of 100 mV/s; (c) charge/discharge curves of PANI/rGO at different current densities; (d) charge/discharge curves of rGO, pure PANI and PANI/rGO at 1A/g; (e) cycling performance of PANI/rGO at 1 A/g for 1000 cycles and 100 mV/s for 10000 cycles; (f) EIS of the PANI and PANI/rGO.

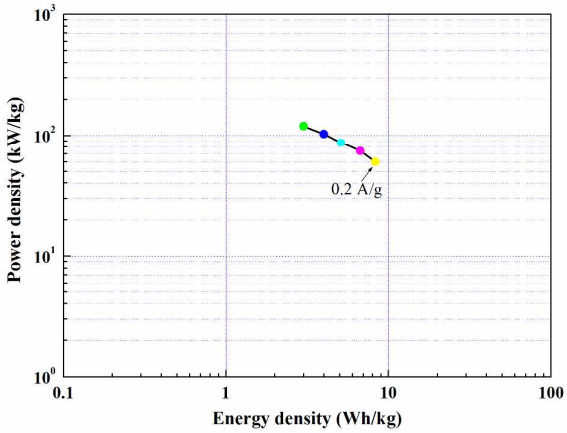

Fig.5 The Ragone plot of energy density versus power density for the PANI/rGO at different charge/discharge current densities.